Benajes Calvo, JV.; Novella Rosa, R.; Pastor Enguídanos, JM.; Hernández-López, A.; Hasegawa, M.; Tsuji, N.; Emi, M.... (2016). Optimization of the Combustion System of a Medium Duty Direct Injection Diesel Engine by Combining CFD modeling with Experimental Validation. Energy Conversion and Management. 110:212-229. doi:10.1016/j.enconman.2015.12.010.

Optimization of the Combustion System of a Medium Duty Direct Injection Diesel Engine by Combining CFD modeling with Experimental Validation

Jesus Benajes, Ricardo Novella*, Jose Manuel Pastor, Alberto Hernández-López
CMT-Motores Térmicos
Universitat Politècnica de València
Camino de Vera s/n, 46022, Valencia (Spain)

Manabu Hasegawa, Naohide Tsuji, Masahiko Emi, Isshoh Uehara
Nissan Motor Co., Ltd.
6-1, Daikoku-cho, Tsurumi-ku, 230-0053, Yokohama (Japan)

Jordi Martorell, Marcos Alonso
Nissan Technical Centre Europe-Spain
Zona franca sector B C/3 77-111, 080540, Barcelona (Spain)

Abstract

The research in the field of internal combustion engines is currently driven by the needs of decreasing fuel consumption and CO_2 emissions, while fulfilling the increasingly stringent pollutant emissions regulations. In this framework, this research work focuses on describing a methodology for optimizing the combustion system of compression ignition (CI) engines, by combining computational fluid dynamics (CFD) modeling, and the statistical Design of Experiments (DOE) technique known as Response Surface Method (RSM). As a key aspect, in addition to the definition of the optimum set of values for the input parameters, this methodology is extremely useful to gain knowledge on the cause/effect relationships between the input and output parameters under investigation.

This methodology is applied in two sequential studies to the optimization of the combustion system of a 4-cylinder 4-stroke Medium Duty Direct Injection (DI) CI engine, minimizing the fuel consumption while fulfilling the emission limits in terms of NO_x and soot. The first study targeted four optimization parameters related to the engine hardware including piston bowl geometry, injector nozzle configuration and mean swirl number (MSN) induced by the intake manifold design. After the analysis of the results, the second study extended to six parameters, limiting the optimization of the engine hardware to the bowl geometry, but including the key air management and injection settings. For both studies, the simulation plans were defined following a Central Composite Design (CCD), providing 25 and 77 simulations respectively.

The results confirmed the limited benefits, in terms of fuel consumption, around 2%, with constant NO_x emission achieved when optimizing the engine hardware, while keeping air management and injection settings. Thus, including air management and injection settings in the optimization is mandatory to significantly decrease the fuel consumption, by around 5%, while keeping the emission limits.

Keywords:

Diesel Engine, CFD model, Engine Optimization, Engine Efficiency, Emissions control

* *Corresponding author*
Email: rinoro@mot.upv.es
Phone: (0034) 96 387 76 55 // Fax: (0034) 96 387 76 59

1. Introduction

Research on combustion systems in the frame of Internal Combustion Engines (ICE) for road and rail transport applications is traditionally focused on optimizing the conventional and also the advanced combustion concepts for accomplishing the pollutant emissions standards. Those standards are becoming more difficult to achieve, while increasing the engine thermal efficiency arises an additional objective in order to decrease fuel consumption and then CO_2 emissions. Nowadays, engines provide a good trade-off between pollutant emissions and fuel consumption since they are already optimized, so developing them to reach further improvements becomes a hard task.

Experimental optimization is a well-known method due to the simplicity of adjusting air management, injection setting or fuel composition aiming for a better combustion process. Therefore, in the past years most of the research works in the field of diesel engine analysis and optimization focused on the injector and combustion chamber design, or even the use of fuels with different properties, have been performed experimentally. Choi et al [1] studied the effect of the bowl geometry and a double row nozzle with 12 holes on the emissions. Atmanli et al [2] used a Response Surface Method for finding the optimum diesel-n-butanol-cotton oil ternary blend ratios also for controlling emissions. This experimental approach has been widely applied also to the analysis and optimization of advanced combustion concepts. Genzale et al [3] measured how the emissions are affected by the chamber geometry operating with the low temperature combustion (LTC) concept. Benajes et al [4] investigated the potential of the piston geometry to improve the results provided by the Reactivity Controlled Compression Ignition (RCCI) concept in terms of combustion efficiency and emissions. However, the experimental optimization of parameters related to the engine hardware, such as the combustion chamber or the injector geometry is costly in terms of time and resources since it involves piston or injector manufacturing and assembling, together with weeks or even months of intensive testing.

Recently, Computational Fluid Dynamics (CFD) is gaining reliability in predicting emissions and combustion characteristics by using properly calibrated and validated models. Then, CFD modeling is a very interesting alternative compared to the experimental approach especially for the optimization of the engine hardware due to its lower requirements in terms of time and resources. Thus, it is worth to develop an optimization methodology based on CFD modeling suitable for not only defining the optimum engine hardware/settings configuration, but also to identify qualitatively and quantitatively the most relevant effects of the variables to be optimized (inputs).

Different studies have been carried out using evolutive methods with really encouraging results related to optimum geometries [5,6] or injection and air management settings [7,8,9,10,12]. These results confirm the suitability of genetic algorithms to find the optimum engine configuration (hardware and/or settings), and how the increasing computational power decreases the time cost of combustion chamber optimization until reasonable values. Without these methods, optimization can be carried out by simply discretizing the variables and performing CFD calculation on every combination of them, nonetheless, this limits the amount of parameters to optimize what leads to simple geometries defined by 1 or 2 parameters. Gafoor and Gupta [11] optimized a bowl geometry defined by a single parameter together with the swirl by simulating 35 combinations of them. However, when talking about highly accurate results the amount of iterations required by these evolutive methods to obtain the real optimum (not just a local optimum) are possibly unpredictable and even unacceptable due to the large initial population needed to obtain accurate results [16,17]. Even with the micro-genetic algorithm that requires populations of only 5 individuals, the number of simulations required to reach the optimum is not comparable with RSM methods. Yun and Reitz [14] needed 120 iteration for 4 control parameters and Kim et al. [15] needed 150 iterations for 5 parameters compared to 25 and 43 simulations required for a 4 and 5 parameters RSM. As a result, these evolutive methods demand many resources in terms of CPU and time, especially when simulating 3D combustion chambers for industrial purposes where that increase in the number of simulations implies months. In addition, as previously commented, the exact number of iterations required for a genetic algorithm optimization is unknown forehand since the termination point is arbitrary in order to assure not obtaining a local optimum from the process, so the number of iterations increases drastically.

Traditionally, evolutive methods have been the preferred option to carry out a CFD optimization of ICE, and particularly Compression Ignition (CI) engines. As an alternative, the non-evolutive methods provide a predefined number of iterations that increases with the number of inputs, but for a number of inputs ranging between 4 and 6 the total time cost is still lower than that provided by the genetic algorithms, and different studies applying non-evolutive methods have proven their potential. The high reliability and accuracy in the results that the non-evolutive Response Surface Methods (RSM) provide in a CFD optimization is shown in those studies [18,19,21]. Compared to the evolutive methods, the RSM allows obtaining trends and results in any region of the chosen optimization region with the optimized configuration. Those trends can be also obtained using a genetic algorithm after carrying out further post-processing activities, but even in this case the accuracy is lower than that provided by RSM due to the randomness of the training points. Finally, the RSM method has been even applied for other applications as the vehicle on board control of the engine settings to optimize the combustion process [20].

In this framework, the research work reported in the present paper focuses on describing and applying a new methodology for optimizing the combustion system of CI engines based on the RSM approach. The optimization process carried out in this paper is divided in 2 stages, the first one optimizes 4 inputs (2 related to the combustion chamber geometry, swirl number and nozzle included angle (NA)), with results in 25 simulations and the second one considers 6 inputs (2 related to the combustion chamber geometry, 2 related to injection settings and 2 related to air management settings), with results in 77 simulations. From the considerations in this paper, it can be deducted that results generated following this methodology provided much more information and accuracy than a similar optimization using evolutive methods limited to the same number of simulations.

2. Experimental tools

Engine characteristics

The experimental data required for the calibration and validation of the CFD model was obtained from a 4-cylinder 4-stroke Medium Duty Direct Injection (DI) CI engine, equipped with a common-rail injection system. Table 1 contains the main engine characteristic, while Table 2 shows the key settings for the reference operating condition.

Table 1 - Engine main characteristics

Engine data	
Max Torque	550 Nm (1400rpm --2200 rpm)
Max Power	128 kW (2200 rpm)
Combustion Chamber	Re-entrant
Bore x stroke [mm]	96 x 102
Bowl width [mm]	62.4
Unitary Displacement [cm^3]	738.3
Connecting rod length [mm]	154.5
Geometric compression ratio [-]	15.5
Nozzle hole number	9

Table 2 - Engine operating conditions

Operating conditions			
Speed [rpm]	1200	1600	1800
Fuel mass [Kg/s]	2.71e-4	9.36e-4	1.50e-3
IMEP [bar]	6.5	16.2	24.9
EGR [%]	17.7	13	11.3
Global equivalence ratio [-]	0.6	0.73	0.75
Intake temperature [K]	324.9	313.15	318.9
Boost pressure [bar]	1.15	2.28	3
MSN [-]	2	2	2

Test cell characteristics

The engine is assembled into a fully instrumented test cell. An external compressor provides the intake air (oil and water-free) required to simulate boost conditions, while the exhaust backpressure is reproduced and controlled by means of a throttle valve placed in the exhaust line after the exhaust settling chamber. The experimental facility also includes a high pressure EGR system, designed to provide arbitrary levels of cooled EGR.

The test cell is equipped with a dedicated air and fuel flow meters, and a set of temperature and pressure sensors to assure the proper operation of the system. Data of O_2, CO, CO_2, HC, NO_x, N_2O and exhaust gas recirculation (EGR) rate is measured with a state-of-the-art exhaust gas analyzer, while Smoke emissions in Filter Smoke Number (FSN) units are measured by a Smokemeter connected to the exhaust line. Instantaneous high frequency signals such as cylinder pressure, pressures at the intake and exhaust ports and energizing current of the injector are sampled with a resolution of 0.2 crank angle degree (degree to top dead center). Cylinder pressure is measured using a state-of-the-art piezoelectric sensor. The most important combustion parameters like indicated mean effective pressure (IMEP), maximum cylinder pressure (P_{max}), pressure gradient (dP/da), combustion noise, combustion phasing angles and heat release rate (HRR); as well as the initial thermodynamic conditions and wall temperatures required for performing the setup of the CFD model, are calculated from the experimental cylinder pressure signal by means of the in-house combustion analysis software (CALMEC) [22,23]. This 0-Dimensional model simplifies the phenomena occurring inside the engine cylinder, so it does not provide any information related to local thermochemical conditions. However, the instantaneous evolution of the energy released by the progress of the combustion can be obtained with accuracy by resolving the first law of thermodynamics taking the combustion chamber as the control volume independently from the local conditions where this energy is being released.

Table 3 Accuracy of the instrumentation used in this work

Variable measured	Device	Manufacturer/model	Accuracy
In-cylinder pressure	Piezoelectric transducer	Kistler/6125B	±1.25 bar
Intake/exhaust pressure	Piezorresistive transducers	Kistler/4045A10	±0.025 bar
Temp in settling chambers/manifolds	Thermocouple	TC direct/type K	±2.5 °C
Crank angle, engine speed	Encoder	AVL/364	±0.02 deg
NO_x, CO, HC, O2, CO2	Gas analyzer	HORIBA/Mexa 7100 DEGR	4%
FSN	Smoke meter	AVL/415	±0.025 FSN
Diesel fuel mass flow	Fuel balances	AVL/733S	±0.2 %
Air mass flow	Air flow meter	Elster/RVG G100	±0.1 %

Injection rate test rig

Measurements of injection rate were carried out with an Injection Discharge Rate Curve Indicator (IRDCI) commercial system. The device makes it possible to display and record the data that describe the chronological sequence of an individual fuel injection event. The measuring principle used is the Bosch method [24], which consists of a fuel injector that injects into a fuel-filled measuring tube.

The fuel discharge produces a pressure increase inside the tube, which is proportional to the increase in fuel mass. The rate of this pressure increase corresponds to the injection rate. A pressure sensor detects this pressure increase, and an acquisition and display system further processes the recorded data for further use.

3. Modeling tools

The section below describes the experimental and theoretical tools used to carry out the research. This brief description focuses only on their most relevant characteristics.

CFD model

The StarCD code version 4.18 [25] was used to perform the CFD simulations of the engine combustion system. The axisymmetry of the combustion chamber allow us to create a sector mesh comprising 131360 cells at BDC with periodic boundary conditions after performing a grid convergence study. Each case was calculated as a closed cycle combustion, this is from the closure of the inlet valves to the opening of the exhaust valves (from 246.8 to 463° aTDC with the TDC at 360 deg). The simulations were calculated with 12 cores each with an average time cost of 36 hours per simulation.

The combustion model was the ECFM-3z from IFP [26]. Concerning pollutants, NO_x were calculated using the extended Zeldovich (thermal) mechanism, where source terms were obtained from a flamelet library [27]. A two-step Hiroyasu-like model was used for soot formation and oxidation [28].

Concerning the physical sub-models, the diesel spray was simulated with the standard Droplet Discrete Model available in StarCD. Spray atomization and break-up were simulated by means of the Huh-Gosman [29] and Reitz-Diwakar [30] models, respectively. Diesel fuel physical properties were given by the DF1 fuel surrogate [31].

In these simulations, turbulent flow was modelled by means of the RNG k-ε model [32], with wall-functions based on the model from Angelberger [33] in order to account for wall heat transfer. An implicit scheme was used for time discretization, while divergence terms used the second order Monotone Advection and Reconstruction Scheme (MARS) [25]. Velocity-pressure coupling was solved by means of a Pressure-

Implicit with Splitting of Operators (PISO) algorithm [34]. The reference values used for the boundary and initial conditions are shown in Table 4.

Table 4 - Cylinder thermodynamic conditions at IVC & combustion chamber mean wall temperatures.

Speed [rpm]	P_{IVC} [bar]	m_{IVC} [g]	T_{IVC} [K]	Y_{O2} [%]	Y_{N2} [%]	Y_{CO2} [%]	Y_{H2O} [%]	T_{wpis} [K]	T_{wliner} [K]	T_{whead} [K]
1200	1.62	0.86	407	19.88	76	2.85	1.26	425.3	380.1	415.8
1600	3.48	1.77	425	20.06	76.04	2.7	1.2	507.4	406.8	496.8
1800	4.67	2.33	434	20.2	76.07	2.58	1.14	551.9	425.9	546

These reference values could not be kept constant for all the simulations due to having EGR and boost pressure as optimization parameters, what has a huge impact on the air composition and thermodynamic conditions and therefore, they were accordingly adjusted in each simulation, assuming constant volumetric efficiency and T_{IVC}. In a similar way, the calculation of the high pressure loop IMEP in the post-processing is affected by these variations. The IMEP of the closed cycle can only be compared against experimental data in relative values, so in order to compare in absolute values, the pressure profiles from bottom dead center (BDC) to intake valve closing (IVC) and from exhaust valve opening (EVO) to BDC were taken directly from experimental results, and adjusted in each simulation according to the corresponding operating conditions.

Bowl geometry model

The generation of the combustion chamber geometry is one of the most time consuming step in an optimization. Bowl shapes are very diverse, which makes it difficult to be adjusted, especially with only a few parameters. However, in order to capture properly the trends of the geometric parameters in the RSM method, the process needs to be consistent, this is, the restrictions of the original bowl have to be maintained. For that reason, an in-house code to adjust and resize any bowl contour was developed The basic idea behind the code is to adjust the original geometry with Bezier curves and then readjust the curves iteratively taking into account the restrictions, like for example the maximum width of the bowl is limited by the oil gallery location. Figure 1 shows the reference bowl, adjusted with Bezier curves and compared with variations of the geometry for different values of the geometric parameters.

The Bezier line and control points used to adjust the original bowl can be seen in the figure and it is noticeable how the adjusted profile reproduces the original shape perfectly and the new generated lines, because of the restrictions imposed, keep the main aspects of the bowl.

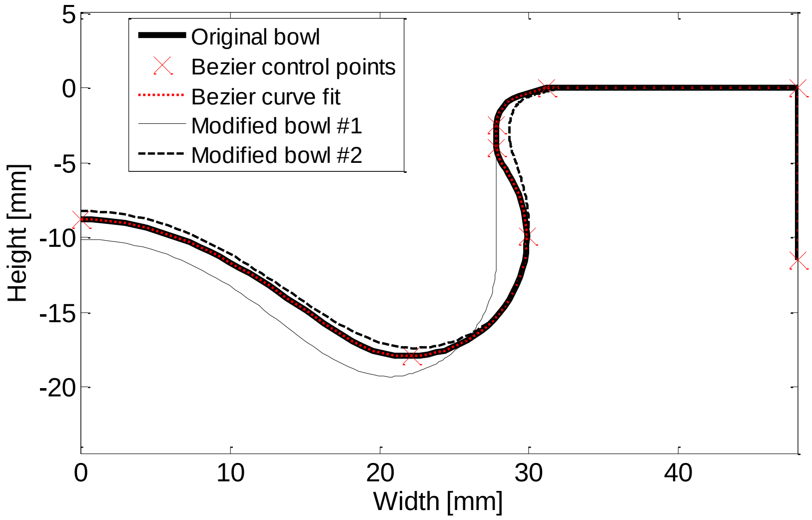

Figure 1 - Bowl geometry profiles: the original bowl with the Bezier polynomial and control points and two examples of newly-generated bowl.

Injection rate model

The injected fuel mass flow rate profile has a critical effect on the combustion process so in order to be consistent with the experimental data, an in-house 0D model code capable of reproducing any injection rate profile was developed. The model needs experimental data because a measured injection rate profile has to be adjusted using Bezier curves and then, the curve generated from adjusting the experimental injection rate profile is modified to fit the required injection pressure and total injected mass. Figure 2a shows the measured injection profile used as reference and the curves obtained from the software and Figure 2b shows the readjusted injection profile and the corresponding experimental data.

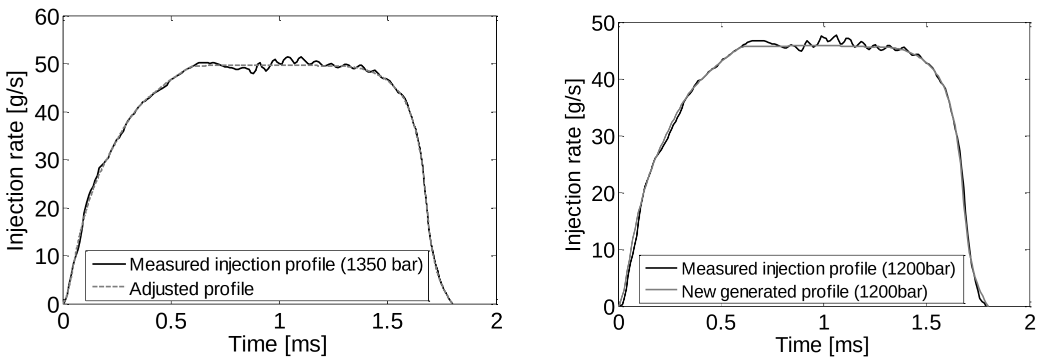

Figure 2 a) Reference injection profile at 1300bar and adjusted curve with Bezier curves. b) New generated profile with the 0D model at 1200bar and the experimental data for 1200bar.

A critical aspect of the injection is the slope of the injection rate when the injector receives the electric signal and when the signal ends. It can be seen in Figure 2 how the injection profile generator keeps the original slopes, what assures the consistency with the experimental data.

4. Methodology

Accuracy is one of the most difficult aspects when optimizing unknown processes that cannot be tested experimentally. Part of this inaccuracy comes from the CFD model but an important fraction also comes from the optimization methodology. In order to avoid uncertainties due to the combustion process and to be able to validate the methodology, the ranges of the optimization parameters were chosen in order to keep a conventional combustion in all cases so the know-how on this combustion models can be used to validate results and trends.

The methodology described in this section has 3 steps, while each of them has their own tools, which are described in the tools section. Figure 3 shows summarizes the 3 steps of the methodology.

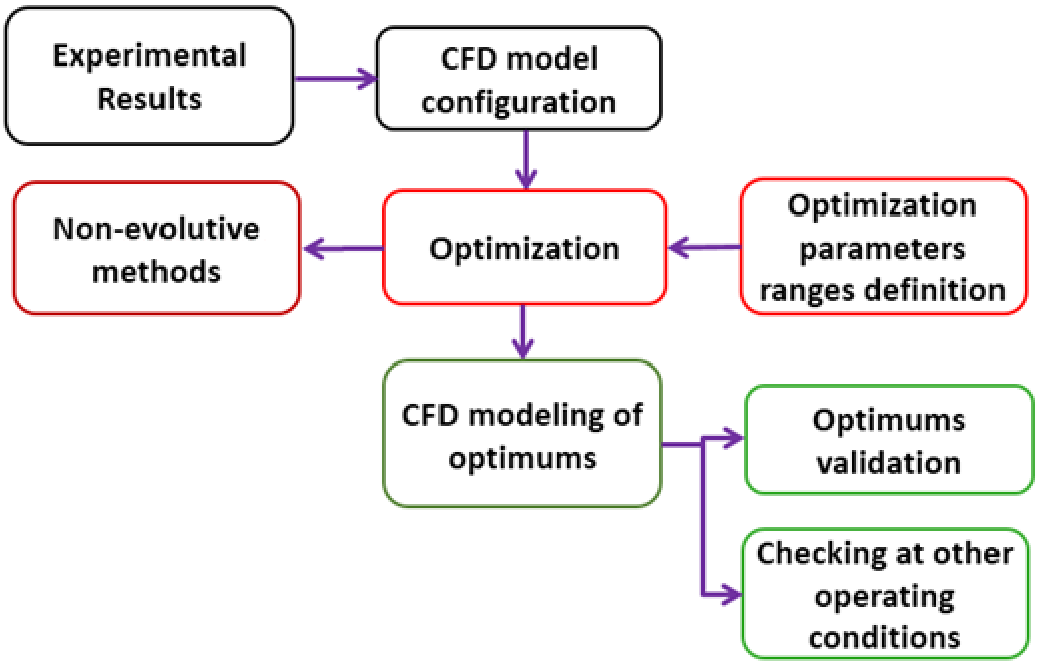

Figure 3 Flow chart of the methodology steps

The first step is the configuration of the CFD model used for the later optimization. It has to be properly calibrated and validated with experimental data because the main objective of the optimization process is to vary parameters in a given range so not having a well calibrated model could change the trends provided by the engine. It has to be pointed that the calibrated model parameters have been kept constant for the following steps.

The second step is dedicated to the optimization of the combustion system. The methodology for this optimization is based on Design of Experiments (DOE) techniques, particularly the Response Surface Method (RSM). This method was selected due to its attractive cost/benefit ratio specially compared to the evolutive optimization methods, which are more costly and less predictable in terms of time. Moreover, due to the randomness of the simulated points, with evolutive methods it is more difficult and less accurate to capture the cause/effect relations between the input and the output parameters.

The final step focuses on validating the optimums. Once the DOE are performed, a series of convenient optimum are obtained from the response surface and those optimums have to be validated with the CFD model to assure the wanted accuracy of the method. Additional validations at other operating conditions are necessary to check if the new set up has a better performance than the original in well-representative points of the engine map.

In this study, four parameters for Stage 1 and six parameters for Stage 2 were chosen to be optimized and a Central Composite Design (CCD) defined the DOE test plan with 25 and 77 simulations respectively. Among the output parameters, efficiency, emissions and combustion related parameters were included. The objective of some of these parameters was to confirm the key trends followed by the main outputs.

Concerning the input factors, the bowl geometry was parameterized by means of two geometrical relations, the ratio between the rip bowl diameter (d) and the cylinder bore (B) and a second parameter (K) defined specifically to control the reentrant shape of the bowl avoiding the artificial generation of extremely deformed bowl shapes. Due to its definition, included in Figure 4 together with the geometry of the central point of the DOE, the higher the K the more reentrant bowl shape. The ranges for the input parameters kept for all DOE are shown in Table 5 and Table 6.

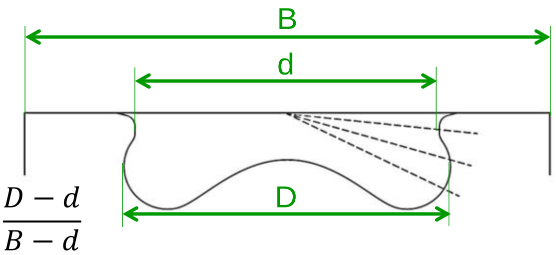

$$K = \frac{D - d}{B - d}$$

Figure 4 – Sketch of the bowl geometry for the central point of the DOE and definition of K factor.

Table 5 - Ranges for the input factors for the optimization Stage 1 DOE of 4 parameters.

	d/B [-]	**K [-]**	**Swirl [MSN]**	**NA [deg]**
Ref	0.57	0.14	2	148
min	0.53	0	0.5	140
max	0.63	0.2	2.5	156

Table 6 - Ranges for the input factors for the optimization Stage 2 DOE of 6 parameters.

	GEOMETRY		AIR MANAG.		INJECTION	
	d/B [-]	K [-]	P2 [bar]	EGR [%]	IP [bar]	SoI_m [deg a TDC]
Ref	0.57	0.14	2.28	13	1230	359.5
min	0.53	0	2.28	13	1200	355.5
max	0.63	0.2	2.48	23	1600	361.546

Figure 5 contains the combinations of the 2 parameters related to the bowl geometry included in the DOE design compared to those of the original engine bowl geometry. The same comparison is carried out between the other settings modified in the optimization process.

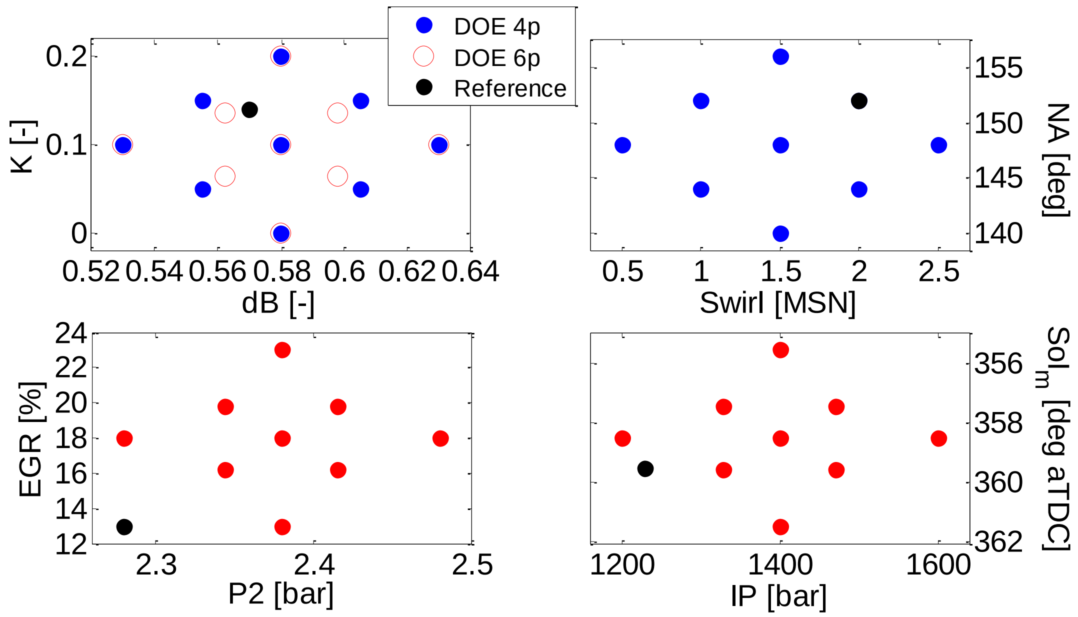

Figure 5 - Combinations input parameters for Stages 1 and 2.

It is important to highlight how despite the well-known trade-off existing between ISFC and BSFC especially when the boost pressure is adjusted, the analysis was carried out considering ISFC and not BSFC since this research focuses on understanding the requirements of the combustion system to optimize the energy conversion from heat to work respecting emission constraints. These processes are intrinsically controlled by the combustion process, while the mechanical losses (including pumping losses) are not accounted for since they depend on external factors not directly controlled by the combustion process such as the lubrication and surface finish (friction losses), the mechanical efficiency of auxiliary systems (auxiliary losses) or the turbocharging system efficiency and its matching (pumping losses). The optimization of the combustion system to obtain the best indicated efficiency carried out in this investigation must be followed by a next step dedicated optimization of the engine subsystems to transfer the ISFC improvements into final BSFC benefits.

5. Results and discussion

The section below describes the CFD model validation and two optimizations performed for the reference engine. The first optimization stage focuses on optimizing four engine parameters (bowl shape, intake manifold design and injection hardware) and the second stage keeps the geometric parameters as optimization inputs and adds four more optimization parameters (injection and air management settings).

5.1. CFD model calibration and validation

The CFD model was thoroughly validated by simulating the three operating conditions under investigation described in Table 2. The results of the CFD model compared against the experimental data in terms of performance and pollutants after calibrating the sub-model constants, especially those related to the soot model, are included in Figure 6, Figure 7 and Figure 8.

Those figures show a fair agreement in terms of performance (IMEP), fuel consumption (ISFC) and combustion characteristics (HRR). In addition, the final soot levels were close to experimental data after adjusting the constants of the soot formation model. An over-prediction of NO_x values is observed for the high load condition, probably related with the faster rise on the main HRR compared to experimental data, however, the quality of the CFD model was considered as suitable for carrying out the optimization activities.

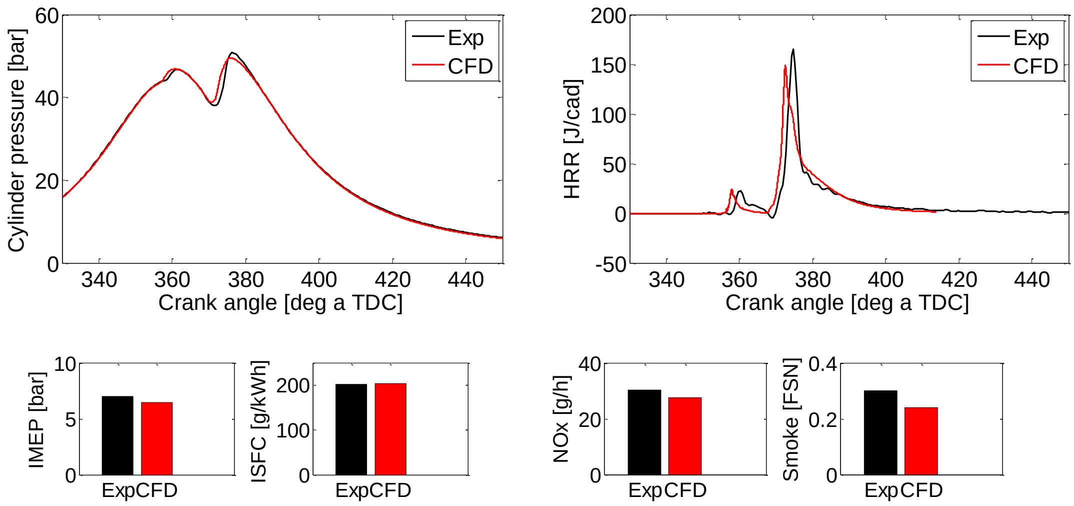

Figure 6 – Experimental vs CFD results with the reference combustion system at 1200 rpm

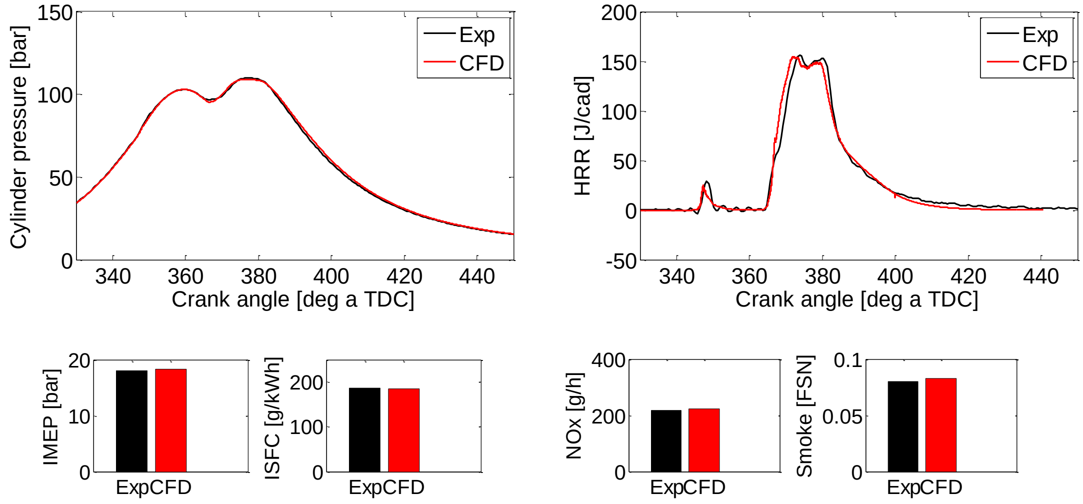

Figure 7 - Experimental vs CFD results with the reference combustion system at 1600 rpm

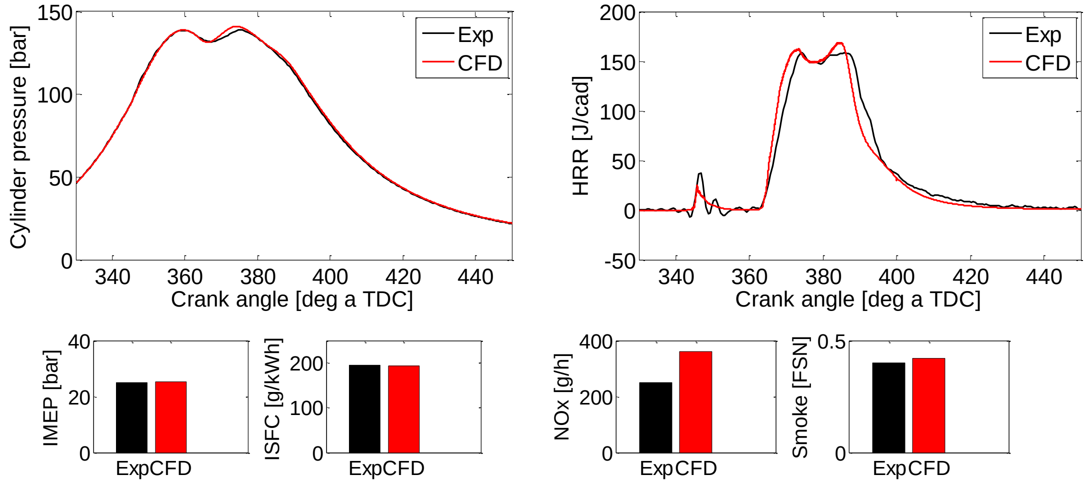

Figure 8 - Experimental vs CFD results with the reference combustion system at 1800 rpm

5.2. Optimization Stage 1

A preliminary optimization process was carried out with the aim of investigating the impact of the engine hardware and nozzle configurations on emissions and fuel consumption. This first stage focused on medium speed/load, evaluating later the optimum configurations at low speed/load and high speed/load operation conditions.

Air management and injection settings were kept constant at their reference values. Then, a double shot injection (pilot plus main events) at the reference timings and injection pressure was considered. The engine volumetric compression ratio was also kept constant at the reference value shown in Table 1.

Four parameters related to the bowl shape (diameter and re-entrant profile), intake manifold design (swirl) and injection hardware (nozzle included angle) were optimized by means of the DOE technique known as Response Surface Method. The ranges of these optimization parameters were shown in Table 5. Additional details of the response surface functions can be found in Annex 1.

Figure 9 and Figure 10 show the effects of bowl geometry (d/B and K) and the effects of swirl and nozzle included angle (NA) respectively on the end of combustion angle (CA90abs), engine efficiency (ISFC) and NO_x -Smoke emissions.

Focusing on the main general trends observed in Figure 9, it can be seen how increasing bowl diameter (d/B) results in a later CA90abs while the effect on ISFC is almost negligible. The impact on NO_x and Smoke emissions was moderate. Additionally, increasing the reentrant shape of the bowl (K) clearly advances the end of combustion (CA90abs) and decreases ISFC independently from the combination of the other input factors. NO_x emissions increase while Smoke was much less affected.

Switching to the most relevant trends observed in Figure 10, increasing swirl advances CA90abs and decreases ISFC also independently from the values of the other input parameters. NO_x and Smoke increase and decrease respectively. Finally, increasing the nozzle included angle results in similar trends than those observed increasing swirl, so wide angle nozzle provided better results in terms of ISFC and Smoke emissions.

On the light of the results, Table 7 describes the two optimum combustion systems defined following two different optimization paths:

1. Minimizing ISFC keeping the NO_X-Smoke trade-off (S1 Opt1)
2. Improving the NO_x -Smoke trade-off accepting 2% ISFC penalty (S1 Opt2).

The optimized bowl profiles compared to that of the reference combustion system are shown in Figure 11, together with the combustion system definition for those optimal configurations. Observing these data, both optimization paths resulted in similar bowl diameter, with d/B around 0.6, but higher reentrant shape, higher K, was required for the minimum ISFC criterion compared to the smaller K for the improving NO_x -Smoke trade-off criterion. In all cases higher nozzle included angle than the reference engine were obtained, especially for the minimum ISFC combustion system configuration.

The two optimized configurations were modeled and compared with the reference engine in Figure 12. It is shown how S1 Opt1 (best ISFC) provided slightly decreased fuel consumption by less than 0.5%, while NO_x slightly increases by +1.4% and the Smoke level is nearly unchanged keeping FSN below 0.1. For S1 Opt 2 (best NO_x -Smoke trade-off) NO_x decreases by 17% with Smoke still below 0.1 FSN at the expense of a minor increment in ISFC by 0.7%, below the acceptable limit. The two optimized configurations were also evaluated for the other two operating conditions, 1800 rpm - high load and 1200 rpm - low load. Results shown in Figure 12 confirm that both combustion systems also work adequately in these other operating conditions.

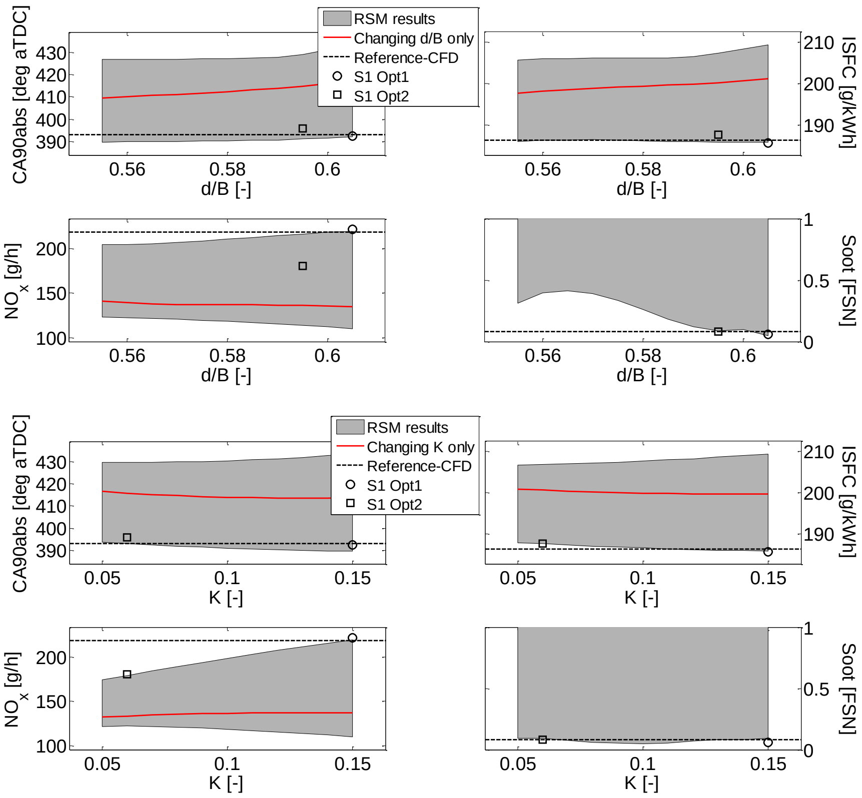

Figure 9 – Effect of d/B (top) and K (bottom) on key combustion, emissions and performance parameters. Reference engine levels are included as red lines.

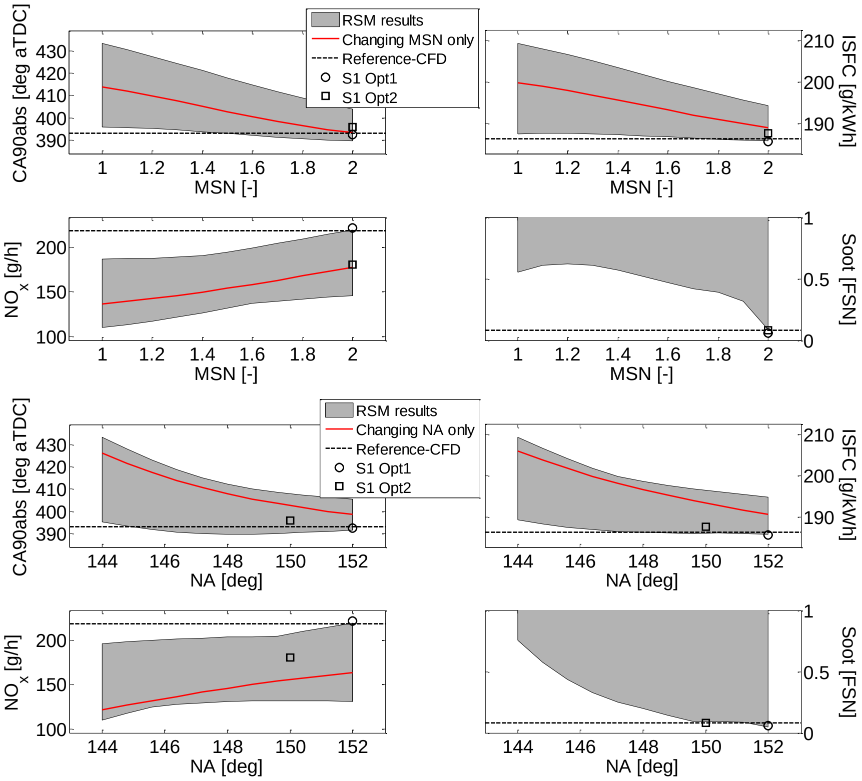

Figure 10 - Effect of swirl (top) and Nozzle included angle (bottom) on key combustion, emissions and performance parameters. Reference engine levels are included as red lines.

Table 7 - Optimized combustion systems after Stage 1.

	d/B [-]	K [-]	Swirl [MSN]	NA [deg]
S1 Opt1 *(best ISFC)*	0.605	0.15	2	152
S1 Opt 2 *(best NO_x-Smoke)*	0.595	0.06	2	150

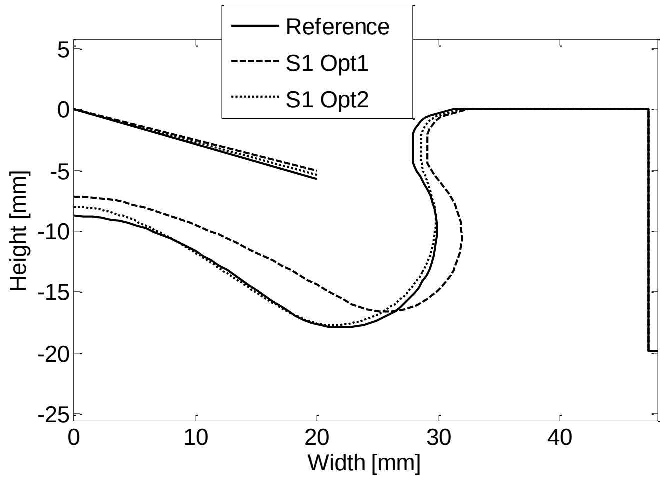

Figure 11 - Optimized combustion systems after Stage 1.

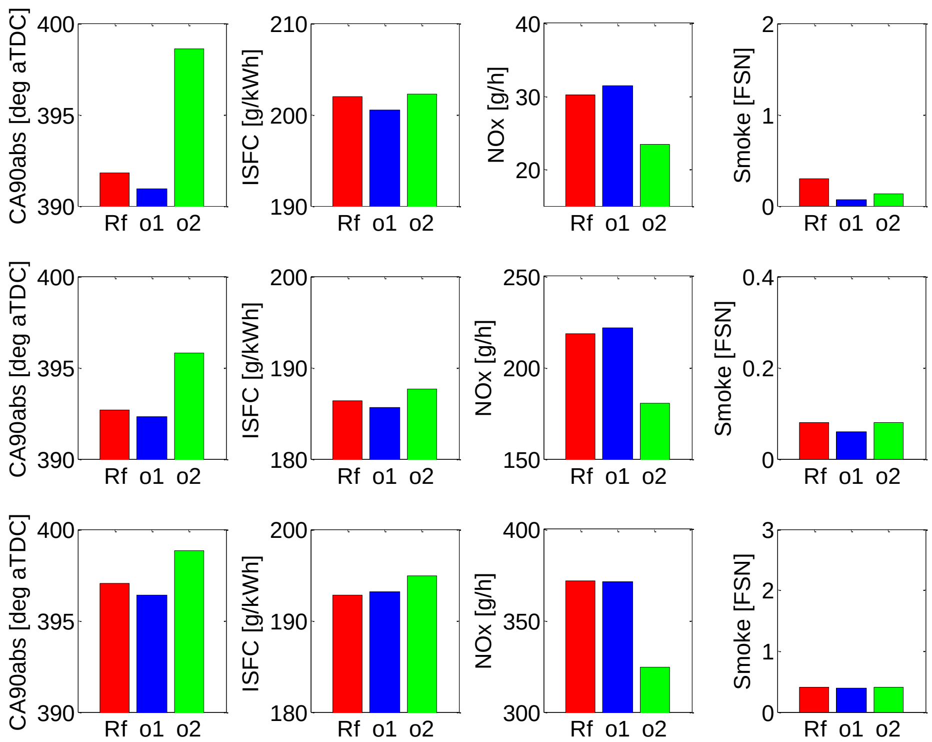

Figure 12 – Stage 1 optimized combustion systems assessment at 1200 rpm – low load (top), 1600 rpm – half load (mid) and 1800 rpm – full load (bottom). Rf refers to the reference combustion system, o1 to the Stage 1 Opt 1 and o2 to the Stage 1 Opt 2 combustion systems

As a key conclusion of this Stage 1, the implementation of the original attractive optimization path based on designing a quiescent combustion system with low swirl and no-reentrant bowl shape, which is expected to improve engine efficiency by reducing the convective heat transfer to the combustion chamber walls, was not possible at least keeping the reference air management and injection settings defined by the current engine technology. Additionally this Stage 1 evidences the low potential of improvement in terms of ISFC while keeping constant emissions attainable by optimizing only the geometry of the engine, supporting the similarity of results between different geometries keeping the same injection and air management setting reported by Rakopoulos et al [13]. This very limited improvement encourages the definition of a second optimization stage adding the key air management (intake pressure and EGR) and injection settings (start of the main injection and injection pressure) for further investigating the potential for ISFC reduction.

5.3. Optimization Stage 2

From the knowledge generated in the previous stage, this Stage 2 focuses on defining a set of optimum combustion chamber, injection settings and air management settings also at the medium speed/load operating condition, evaluating the performance of the optimized combustion systems in the other two operating conditions. Since the maximum number of optimization parameters considered as suitable for the methodology in order to have an acceptable time cost is six, and the reference nozzle angle and swirl level were both quite optimized, only the two geometrical parameters related to the bowl shape (d/B and K) were kept for Stage 2. The detailed information about the parameters included in this optimization together with their ranges is included in the methodology section (Table 6). Additional information concerning the response surface functions can be found in Annex 1.

The impact of the input parameters over the output responses was analyzed in order to establish clear cause/effect relationships. Figure 13 shows the effect of bowl geometry (d/B and K), Figure 14 the effect of air management settings (P2 and EGR) and Figure 15 the effect of injection settings (IP and SoI_m) on the end of combustion angle (CA90abs), ISFC and NO_x-Smoke emissions.

Focusing on the main trends observed in Figure 13, increasing bowl diameter (d/B) clearly delays CA90abs and increases ISFC even compensating its effect by adjusting the other five input parameters. The impact on NO_x and Smoke emissions is moderate and both can be easily controlled. Increasing the reentrant shape of the bowl (K) has moderate impact on CA90abs and ISFC but, contrarily to what was observed in Stage 1, now its effect can be compensated by combining properly the other input factors. NO_x emissions increase while Smoke only increases for highly re-entrant bowl shapes.

Regarding the impact of air management settings shown in Figure 14, increasing P2 results in a slightly earlier CA90abs and then in a reduction in ISFC independently from the values of the other five input parameters. The impact on NO_x and Smoke emissions is moderate and levels below those generated by the reference engine can be easily attained at all P2 levels. Increasing EGR retards CA90abs and then increases ISFC but, on the contrary, NO_x emissions are sharply reduced while Smoke emissions can be controlled by adjusting the other parameters.

Closing this analysis by observing the effects of injection settings included in Figure 15, CA90abs advances and ISFC decreases by increasing IP, and the impact on NO_x and Smoke can be also minimized by adjusting the other input parameters. Advancing SoI_m advances CA90abs and then decreases ISFC. NO_x emissions increase while Smoke can be kept at levels below the reference engine for all SoI_m values.

Results confirm how the bowl shape is strongly coupled to the injector nozzle configuration and, in this case, the nozzle included angle is slightly narrow (148º) and then the optimized combustion systems shifts towards bowls with lower d/B values. Additionally, the path for optimizing ISFC starts by advancing SoI_m to decrease it significantly and introducing the suitable rates of EGR in order to control NO_x emissions keeping a moderate impact on ISFC, while adjusting IP and P2 helps to control Smoke emissions. This path fits with the current trends followed in the field of diesel engine development.

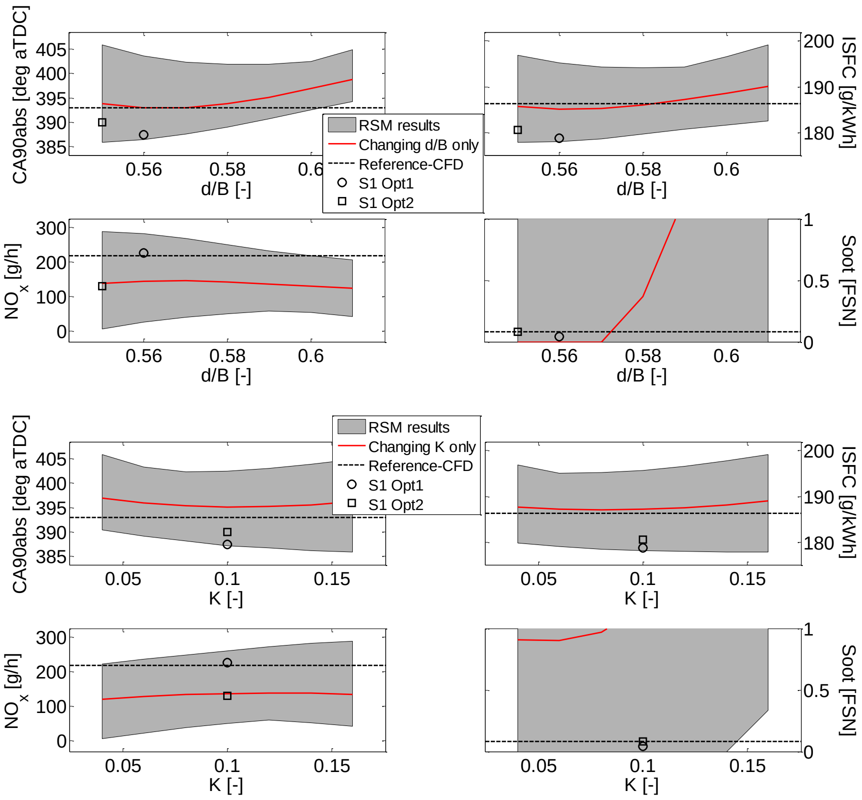

Figure 13 – Effect of d/B (top) and K (bottom) on key combustion, emissions and performance parameters. Reference engine levels are included as red lines.

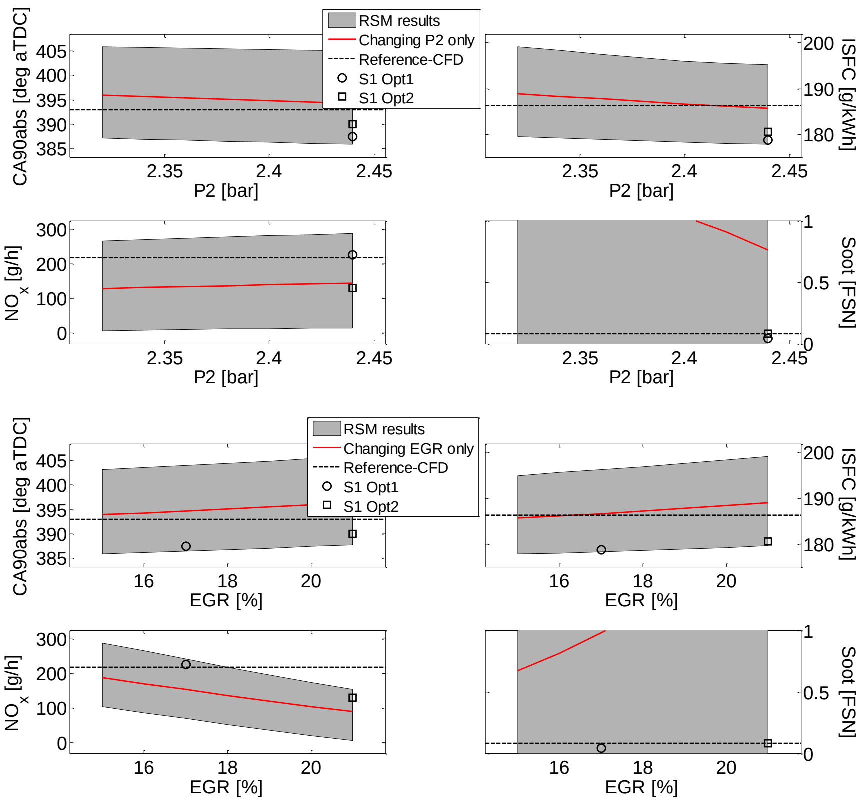

Figure 14 - Effect of P2 (top) and EGR (bottom) on key combustion, emissions and performance parameters. Reference engine levels are included as red lines.

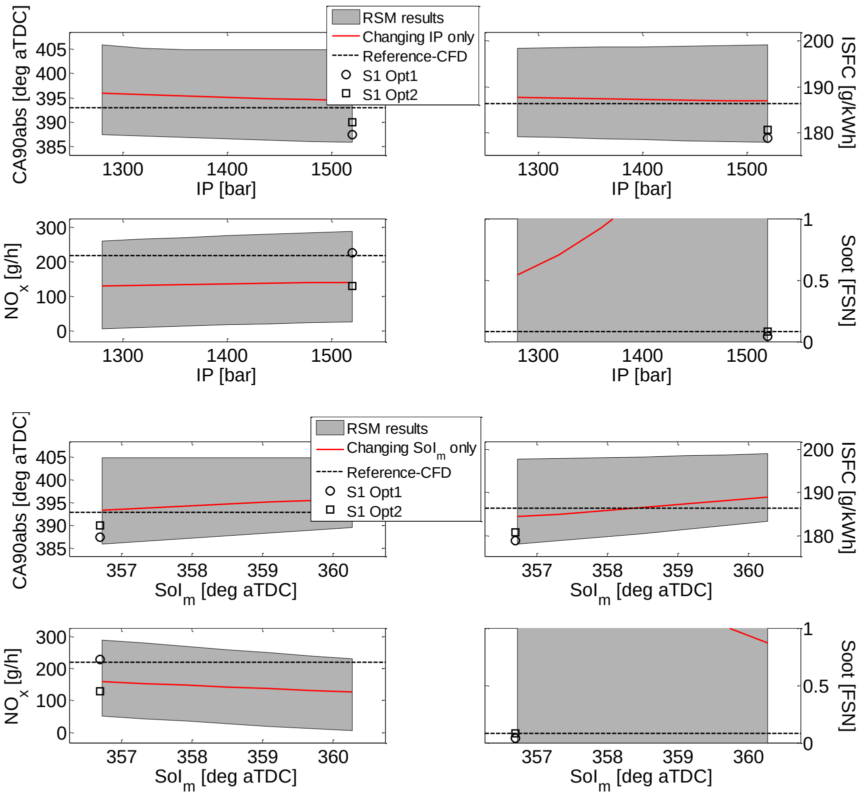

Figure 15 - Effect of IP (top) and SoIm (bottom) on key combustion, emissions and performance parameters. Reference engine levels are included as red lines.

The NO_x -ISFC trade-offs obtained after Stage 1 and Stage 2 included in Figure 16 (left) show the strongly limited potential for optimization provided by modifying only the geometrical parameters (Stage 1), while this potential increases significantly by including the air management and injection settings (Stage 2). However, an important limitation was detected after the analysis of the Stage 2 DOE related to the relation between maximum cylinder pressure (P_{max}) and ISFC observed in Figure 16 (right). It is evident how ISFC is constrained by P_{max}, generating an additional trade-off that must be carefully considered. In fact, the current engine ISFC level cannot be further improved without increasing P_{max} even optimizing the combustion chamber geometry and air management/injection settings altogether.

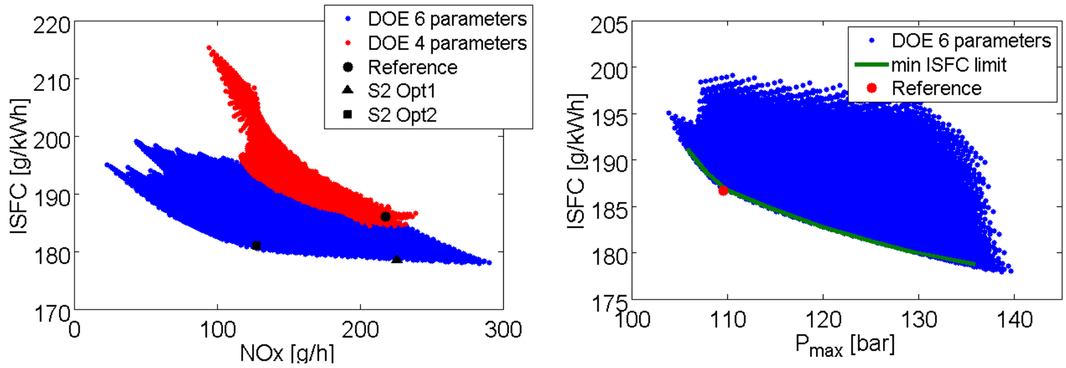

Figure 16 – NO_x and ISFC trade-off for both optimization stages (left). P_{max} and ISFC trade-off detected from the results of the Stage 2 (right).

As in Stage 1, the same two optimization paths were followed for the optimization:

1. Minimizing ISFC keeping the NO_X-Smoke trade-off (S2 Opt1)
2. Improving the NO_x -Smoke trade-off accepting 2% ISFC penalty (S2 Opt2).

The combustion system definitions for those optimal configurations are included in Table 8, and the bowl profiles compared to the reference combustion system and Stage 1 optimums are shown in Figure 17.

Table 8 - Optimized combustion systems after Stage 2

	d/B [-]	K [-]	P2 [bar]	EGR [%]	IP [bar]	SoI_m [deg aTDC]
S2 Opt1 *(best ISFC)*	0.56	0.1	2.44	17	1520	356.7
S2 Opt2 *(best NO_x-Smoke)*	0.55	0.1	2.44	21	1520	356.7

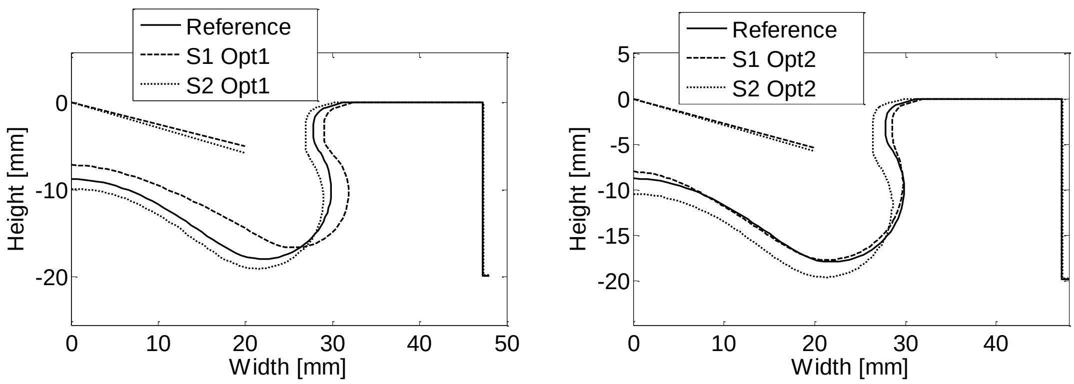

Figure 17 – Optimized piston bowl profiles best ISFC (left) and for best NO_x-Smoke (right). Optimum from Stage 2 and the reference engine have the same NA.

In this Stage 2 the two optimization paths provided quite similar bowl geometries, with d/B 0.56 for best ISFC against 0.55 for best NO_x -Smoke and K equal to 0.1 in both cases. Injection settings were also similar with the highest IP of 1520 bar and the earliest SoI_m of 356.72° aTDC, and they even share the highest P2 equal to 2.44 bar. Therefore, the key difference between both optimization paths is observed in the EGR level, which shifts from 17% for the best ISFC to 21% for the best NO_x -Smoke.

Figure 18 compares the results of the two optimized configurations from Stage 2 with those obtained with the reference combustion system. According to these results, S2 Opt1 and S2 Opt2 decrease fuel consumption by 4.3% and by 3.2% respectively, NO_x slightly increases by 1% for S2 Opt1 but sharply decreases by 43% for S2 Opt2. Smoke level is kept controlled at FSN levels below 0.1 in both cases.

As shown in Figure 18 the optimized combustion systems were also evaluated for the other two operating conditions, 1800 rpm - high load and 1200 rpm - low load using the specific reference setting for each case. The S2 Opt1 combustion system also works adequately under high-load conditions. It is noticeable how the S2 Opt2 improves further the NO_x emissions and keeps a modest reduction in ISFC and soot.

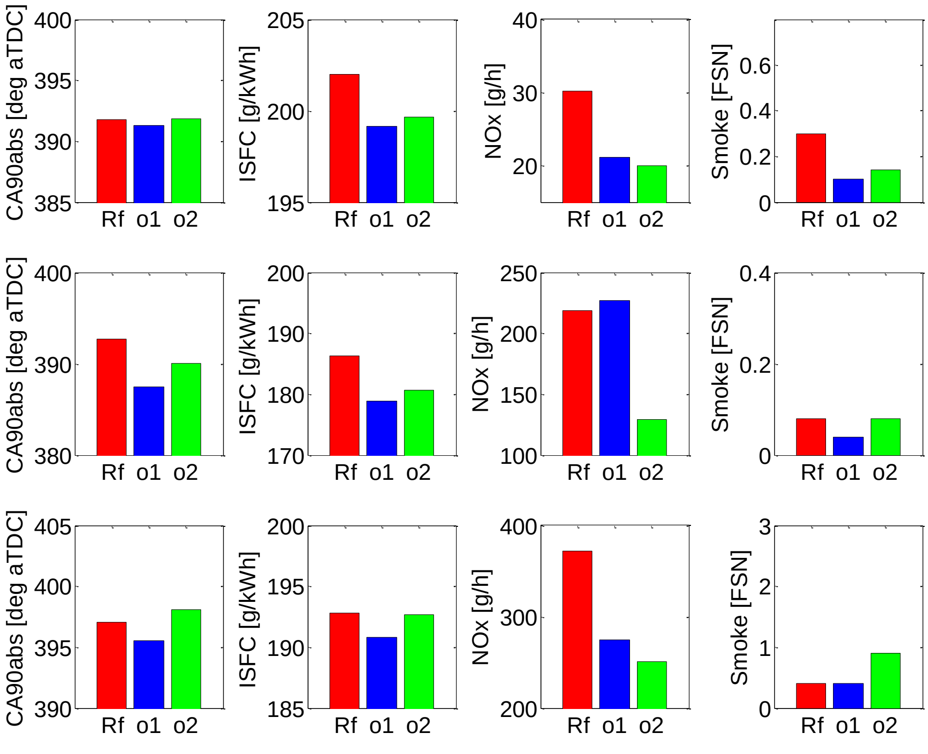

Figure 18 - Stage 2 optimized combustion systems assessment at 1200 rpm – low load (top), 1600 rpm – half load (mid) and 1800 rpm – high load (bottom). Rf refers to the reference combustion system, o1 to the Stage 2 Opt 1 and o2 to the Stage 2 Opt 2 combustion systems

6. Experimental validation

The piston geometries for both optimized combustion systems obtained using the methodology described in this paper were machined and installed in the engine with the aim of validating the quality of the CFD optimization results. The injection and air management settings of the CFD optimums were implemented in order to replicate the exact conditions for both S2 Opt1 and S2 Opt2 combustion systems. Both cases were tested experimentally at medium speed/load and the performance was compared with the CFD results.

Table 9 – Experimental and CFD results for S2 Opt1 and S2 Opt2 at 1600 rpm - medium load.

	ISFC [g/kWh]		**NO_x [g/h]**		**Soot [FSN]**		**dP/da [bar/deg]**	
	EXP	**CFD**	**EXP**	**CFD**	**EXP**	**CFD**	**EXP**	**CFD**
Reference	186.3	187.8 (-0.8%)	218.6	229.8 (+4.9%)	0.08	0.08 (+0%)	4.2	4.3 (+2.3%)
S2 Opt1	177.0	178.3 (+0.7%)	222.7	224.9 (+1.0%)	0.04	0.03 (-33%)	4.5	4.7 (+4.3%)
S2 Opt2	178.9	180.4 (+0.9%)	152.8	146.3 (-4.4%)	0.08	0.09 (11.1%)	4.6	4.6 (+0%)

In general, the agreement is good as indicated in Table 9, confirming how the CFD model setup and the optimization methodology performed well. According to the experimental results, the main objective, ISFC, was reduced by 5% and 4% with S2 Opt1 and S2 Opt2 respectively, fairly similar to the 4.3% and 3.2% predicted by the CFD, while the NO_x and soot were kept constant or improved compared to the reference. In addition, the emission optimum, S2 Opt2, was able to reduce almost 40% NO_x emissions with slightly higher ISFC following also the trends predicted by CFD. Finally, the pressure gradient increases by 10% in both cases, showing a possible noise restriction, what was also captured accurately by the CFD except for a small underprediction with the S2 Opt1.

As a result, the error between the CFD predictions and the experimental validation results is below 3% in the emissions, 2% in ISFC and 5% in noise, proving the robustness and accuracy of the new method.

Following the structure of the paper, the optimum bowls were evaluated at the other operating conditions, 1200 rpm – low load and 1800 rpm – high load, keeping their respective reference settings. However, in the particular case of 1800 rpm – high load the air management and injection settings were slightly re-adjusted to fulfill the mechanical restrictions of the engine along the experiments.

As concluded at the end of optimization Stage 1, the impact of the geometry itself on ISFC is very limited, while the effect on pollutant emission levels is higher, as indicated in Table 10 and Table 11. At the low load case both optimized bowls are able to reduce NO_x emissions by around 15%, keeping ISFC almost constant with less than a 0.5% difference. At the high load case the trend is very similar with a reduction by 6.3% NO_x for S2 Opt1 bowl and by 5% for S2 Opt2 bowl compared to the reference, together with a reduction in ISFC of less than 1% for both optimized bowls. Soot emission levels show little discrepancies that, due to the low value of the experimental measurements, could be explained by experimental errors and/or inaccuracies in the soot model predictions. Nonetheless, the optimum bowl geometries provide competitive soot levels compared to the reference bowl, even following the trends predicted by the modeling results. Focusing now on pressure gradient, it increases by around 18% in the low load case and by 2% in the high load case, also according with the trends previously predicted.

Table 10 – Experimental results for S2 Opt1 and S2 Opt2 at 1200 rpm - low load.

	ISFC [g/kWh]	NO_x [g/h]	Soot [g/h]	dP/da [bar/deg]
Reference	197.72	9.52	0.04	3.92
S2 Opt1	198.23	8.07	0.03	4.79
S2 Opt2	197.52	8.18	0.05	4.5

Table 11 - Experimental results for S2 Opt1 and S2 Opt2 at 1800 rpm - high load.

	ISFC [g/kWh]	NO_x [g/h]	Soot [g/h]	dP/da [bar/deg]
Reference	181.29	103.69	0.02	4.95
S2 Opt1	179.95	94.19	0.07	5.04
S2 Opt2	179.32	98.43	0.05	5.14

As a final remark, these results confirm how the reference bowl geometry was already optimized in terms of ISFC and therefore, the potential for further improvement by re-optimizing the bowl geometry is very limited. As a consequence, air management and injection setting in addition to the bowl geometry must be included in the optimization in order to decrease ISFC by improving the combustion system.

7. Conclusions

An optimization methodology based on a combination of CFD modeling and the statistical Design of Experiments (DOE) technique known as Response Surface Method (RSM) was applied to a 4-cylinder 4-stroke Medium Duty Direct Injection (DI) CI engine in order to reduce ISFC while keeping the main pollutants constant. This methodology provided not only the optimum configurations but also the cause-effect relations between the control and target parameters. This improves the understanding of the requirements of the conventional diesel combustion system and what parameters are more attractive for being optimized.

In a first optimization stage has been found how the combustion system geometry could only improve ISFC by 0.5% without increasing NOx emissions level. This study also indicated that a swirl-supported with re-entrant bowl shape combustion system is still required for this engine and input parameter ranges.

After that, injection and air management settings were included in order to increase the potential of the optimization and to be able to significantly reduce ISFC (around 5%), for constant NO_x emissions, as confirmed by the second optimization stage. It is also noticeable that 40% NO_x reduction can be obtained keeping constant ISFC and soot emissions. Optimization path leads to advanced SoI for improved ISFC, increased EGR in order to control NO_x emissions keeping a moderate impact on ISFC, while adjusting IP and P2 helps to control soot emissions. This path fits with the current trends followed in the field of diesel engine development.

References

1. CHOI, S.; SHIN, S.; LEE, J.; MIN, K.; CHOI, H. *The effects of the combustion chamber geometry and a double-row nozzle on the diesel engine emissions*. Proceedings of the Institution of Mechanical Engineers, Part D: Journal of Automobile Engineering, 2015, vol. 229, no 5, p. 590-598.
2. ATMANLI, A.; YÜKSEL, B.; ILERI, E.; KARAOGLAN, A. D. *Response surface methodology based optimization of diesel–n-butanol–cotton oil ternary blend ratios to improve engine performance and exhaust emission characteristics.* Energy Conversion and Management, 2015, vol. 90, p. 383-394.
3. GENZALE, C. L.; REITZ, R. D.; MUSCULUS, M. PB. *Effects of piston bowl geometry on mixture development and late-injection low-temperature combustion in a heavy-duty diesel engine*. SAE Technical Paper, 2008.
4. BENAJES, J.; PASTOR, J.V.; GARCÍA, A.; MONSALVE-SERRANO, J. *An experimental investigation on the influence of piston bowl geometry on RCCI performance and emissions in a heavy-duty engine*. Energy Conversion and Management, 2015, vol. 103, p. 1019-1030.
5. PARK, S. W. *Optimization of combustion chamber geometry for stoichiometric diesel combustion using a micro genetic algorithm*. Fuel Processing Technology, 2010, vol. 91, no 11, p. 1742-1752.
6. WICKMAN, D. D.; YUN, H.; REITZ, R. D. *Split-spray piston geometry optimized for HSDI diesel engine combustion*. SAE Technical Paper, 2003.
7. SHI, Y.; REITZ, R. D. *Optimization of a heavy-duty compression–ignition engine fueled with diesel and gasoline-like fuels*. Fuel, 2010, vol. 89, no 11, p. 3416-3430.
8. KIM, D.; PARK, S.. *Optimization of injection strategy to reduce fuel consumption for stoichiometric diesel combustion*. Fuel, 2012, vol. 93, p. 229-237.
9. SUN, Y.; REITZ, R. D. *Modeling diesel engine NO_x and soot reduction with optimized two-stage combustion*. SAE Technical Paper, 2006.
10. KOKJOHN, S. L.; REITZ, R. D. *A computational investigation of two-stage combustion in a light-duty engine*. SAE Technical Paper, 2008.
11. GAFOOR, CP A.; GUPTA, R.. *Numerical investigation of piston bowl geometry and swirl ratio on emission from diesel engines.* Energy Conversion and Management, 2015, vol. 101, p. 541-551.
12. GE, H.; SHI, Y.; REITZ, R.; WICKMAN, D.; WILLEMS, W. *Engine development using multi-dimensional CFD and computer optimization*. SAE Technical Paper, 2010.
13. RAKOPOULOS, C. D.; KOSMADAKIS, G. M.; PARIOTIS, E. G. *Investigation of piston bowl geometry and speed effects in a motored HSDI diesel engine using a CFD against a quasi-dimensional model.* Energy Conversion and Management, 2010, vol. 51, no 3, p. 470-484.
14. YUN, H.; REITZ, R. D. *An experimental study on emissions optimization using micro-genetic algorithms in a HSDI diesel engine*. SAE Technical Paper, 2003.
15. KIM, M.; LIECHTY, M. P.; REITZ, R. D. *Application of micro-genetic algorithms for the optimization of injection strategies in a heavy-duty diesel engine*. SAE Technical Paper, 2005.
16. SHI, Y; REITZ, R. D. *Assessment of optimization methodologies to study the effects of bowl geometry, spray targeting and swirl ratio for a heavy-duty diesel engine operated at high-load*. SAE Technical Paper, 2008.
17. SHI, Y.; GE, H.; REITZ, R. D. *Computational optimization of internal combustion engines*. Springer Science & Business Media, 2011.

18. HAJIREZA, S.; REGNER, G.; CHRISTIE, A.; EGERT, M.; MITTERMAIER, H. *Application of CFD modeling in combustion bowl assessment of diesel engines using DoE methodology*. SAE Technical Paper, 2006.
19. YUAN, Y.; LI, G. X.; YU, Y. S.; ZHAO, P.; LI, H. M. *Multi-Parameter and Multi-Object Optimization on Combustion System of High Power Diesel Engine Based on Response Surface Method.* Chinese Internal Combustion Engine Engineering, 2012, vol. 5, p. 005.
20. REITZ, R.; VON DER EHE, J. *Use of in-cylinder pressure measurement and the response surface method for combustion feedback control in a diesel engine*. Proceedings of the Institution of Mechanical Engineers, Part D: Journal of Automobile Engineering, 2006, vol. 220, no 11, p. 1657-1666.
21. LEE, T.; REITZ, R. D. *Response surface method optimization of a high-speed direct-injection diesel engine equipped with a common rail injection system.* Journal of engineering for gas turbines and power, 2003, vol. 125, no 2, p. 541-546.
22. LAPUERTA, M.; ARMAS, O.; HERNÁNDEZ, J. J. *Diagnosis of DI Diesel combustion from in-cylinder pressure signal by estimation of mean thermodynamic properties of the gas.* Applied Thermal Engineering, 1999, vol. 19, no 5, p. 513-529.
23. PAYRI, F.; MOLINA, S.; MARTÍN, J.; ARMAS, O. *Influence of measurement errors and estimated parameters on combustion diagnosis*. Applied Thermal Engineering, 2006, vol. 26, no 2, p. 226-236.
24. BOSCH, W. *The fuel rate indicator: a new measuring instrument for display of the characteristics of individual injection*. SAE Technical Paper, 1966.
25. METHODOLOGY, STAR-CD. Version 4.18. 2012.
26. COLIN, O.; BENKENIDA, A. *The 3-zones extended coherent flame model (ECFM3Z) for computing premixed/diffusion combustion*. Oil & Gas Science and Technology, 2004, vol. 59, no 6, p. 593-609.
27. KARLSSON, A.; MAGNUSSON, I.; BALTHASAR, M.; MAUSS, F. *Simulation of soot formation under diesel engine conditions using a detailed kinetic soot model*. SAE Technical Paper, 1998.
28. HIROYASU, H.; KADOTA, T. *Models for combustion and formation of nitric oxide and soot in direct injection diesel engines*. SAE Technical Paper, 1976.
29. HUH, K. Y.; GOSMAN, A. D. *A phenomenological model of diesel spray atomization*. In Proceedings of the international conference on multiphase flows. 1991.
30. REITZ, R. D.; DIWAKAR, R. *Structure of high-pressure fuel sprays*. SAE Technical Paper, 1987.
31. HABCHI, C.; LAFOSSAS, F. A.; BÉARD, P.; BROSETA, D. *Formulation of a one-component fuel lumping model to assess the effects of fuel thermodynamic properties on internal combustion engine mixture preparation and combustion*. SAE Technical Paper, 2004.
32. YAKHOT, V.; ORSZAG, S. A. *Renormalization group analysis of turbulence. I. Basic theory*. Journal of scientific computing, 1986, vol. 1, no 1, p. 3-51.
33. ANGELBERGER, C.; POINSOT, T.; DELHAY, B. *Improving near-wall combustion and wall heat transfer modeling in SI engine computations*. SAE Technical Paper, 1997.
34. ISSA, R. I. *Solution of the implicitly discretised fluid flow equations by operator-splitting*. Journal of computational physics, 1986, vol. 62, no 1, p. 40-65.

NOMENCLATURE

aTDC	After Top Dead Center
BDC	Bottom Dead Center
CA50	Crank angle for 50% of fuel burnt
CA90	Crank angle for 90% of fuel burnt
CA90abs	Crank angle for 90% of fuel burnt referred to the TDC
CALMEC	In-house combustion analysis software
CCD	Central Composite Design
CI	Compression Ignition
CFD	Computational Fluid Dynamics
d/B	Ratio between the rip bowl diameter (d) and the piston bore (B)
DI	Direct Injection
DOE	Design of Experiments
EGR	Exhaust Gas Recirculation
EVO	Exhaust Valve Opening (angle)
Exp	Experimental
FSN	Filter Smoke Number
HRR	Heat Release Rate
ICE	Internal Combustion Engines
IMEP	Indicated Mean Effective Pressure
IP	Injection Pressure
IRDCI	Injection Rate Discharge Curve Indicator
ISFC	Indicated specific fuel consumption
IVC	Intake Valve Closing (angle)
K	Geometric parameter to control the reentrant shape of the bowl
LTC	Low Temperature Combustion
m	Mass
MARS	Monotone Advection and Reconstruction
MSN	Mean Swirl Number
NA	Nozzle angle
Opt1	Optimum number 1
Opt2	Optimum number 2
P	Pressure
P2	Intake pressure
PISO	Pressure Implicit with Splitting Operators
P_{IVC}	Pressure at IVC
P_{max}	Maximum Cylinder Pressure
RCCI	Reactivity Controlled Compression Ignition
RSM	Response Surface Methods
SoI_m	Start of Main Injection
T	Temperature
TDC	Top Dead Centre
T_{wpis}	Mean Temperature of the piston
T_{wliner}	Mean Temperature of the liner
T_{whead}	Mean Temperature of the head
YO_2	Oxygen concentration in the cylinder
YN_2	Nitrogen concentration in the cylinder
YCO_2	CO_2 concentration in the cylinder
YH_2O	H_2O concentration in the cylinder

Annex 1- Response surfaces functions

The mathematical model used to correlate the optimized input and the outputs of the Stage 1 are shown below.

$$Output = C_1 + db*C_2 + k*C_3 + MSN*C_4 + NA*C_5 + db^2*C_6 + k^2*C_7 + MSN^2*C_8 + NA^2*C_9 + db*MSN*C_{10} + db*k*C_{11} + db*NA*C_{12} + k*MSN*C_{13} + k*NA*C_{14} + MSN*NA*C_{15} + db*k*MSN*C_{16} + db*k*NA*C_{17} + k*MSN*NA*C_{18} + db*MSN*NA*C_{19} + db*k*MSN*NA*C_{20} + MSN^3*C_{21} + db^3*C_{22} + NA^3+C_{23}$$

Where the inputs db, k, MSN and NA as calculated as the example below.

$$db = (db_{value} – (db_{max} + db_{min}) / 2) / ((db_{max} – db_{min}) / 2)$$

being db_{value} the value of db that want to be calculated, db_{max} the maximum value of db in the range used for the optimization and db_{min} the minimum value of db in the range used for the optimization.

The coefficients C1 to C23 are described in Table 12.

Table 12 RSM coefficients for the Stage 1 optimization.

	Mathematical fit coefficients					
Output	P_{max}	dP/da	NO_x	Smoke	ISFC	CA90abs
C_1	106.645	4.277	160.159	2.911	192.207	398.306
C_2	0.809	0.030	5.365	-0.118	0.367	2.625
C_3	1.321	0.005	27.339	-0.806	-2.668	-4.482
C_4	1.438	-0.064	38.838	-4.533	-9.701	-18.410
C_5	0.421	0.003	29.962	-3.121	-8.638	-13.717
C_6	0.513	0.014	3.692	-0.069	0.035	3.724
C_7	1.134	0.016	-8.132	0.659	1.392	4.845
C_8	0.132	0.006	12.259	-0.169	-0.079	3.014
C_9	0.193	0.031	-14.017	1.293	6.670	17.469
C_{10}	1.547	0.041	7.776	-0.485	-2.338	-3.830
C_{11}	-0.523	-0.007	-27.225	2.281	4.958	7.690
C_{12}	0.464	-0.037	23.413	-0.537	-4.443	-8.081
C_{13}	1.462	0.001	17.723	2.436	1.411	2.702
C_{14}	1.278	-0.034	38.268	-1.751	-3.512	-3.262
C_{15}	-1.166	0.016	-21.264	3.060	10.073	19.932
C_{16}	0.023	-0.022	-6.944	0.733	-1.686	-4.781

C_{17}	0.030	-0.020	13.047	-2.269	-3.828	-8.712
C_{18}	-0.586	0.011	-14.584	1.698	1.479	0.082
C_{19}	-0.378	0.005	21.693	-0.588	0.884	5.400
C_{20}	-0.156	-0.040	49.228	-5.027	0.929	4.656
C_{21}	-	-	-12.957	1.496	5.349	10.925
C_{22}	-	-	-18.227	2.481	3.684	3.728
C_{23}	-	-	-4.325	-0.451	-2.468	-6.683

A study of the significance level of the coefficients was performed. The results obtained from the ANOVA for each coefficient is shown in Table 13.

Table 13 Pvalue for all the coefficients used in the RSM for Stage 1

	Pvalues for all coefficients					
Output	P_{max}	dP/da	NO_x	Smoke	ISFC	CA90abs
C_1	0.0000	0.0000	0.0000	0.0000	0.0000	0.0000
C_2	0.0050	0.0020	0.2764	0.0542	0.0501	0.0432
C_3	0.0000	0.0579	0.0031	0.2592	0.0442	0.0328
C_4	0.0000	0.0000	0.0012	0.0007	0.0160	0.0003
C_5	0.0036	0.1753	0.0028	0.0012	0.0118	0.0001
C_6	0.0095	0.0046	0.0182	0.0656	0.6413	0.6588
C_7	0.0068	0.0698	0.0002	0.0226	0.3081	0.5701
C_8	0.0001	0.0072	0.3220	0.0186	0.0386	0.0689
C_9	0.0000	0.2239	0.0159	0.2703	0.0198	0.1567
C_{10}	0.0002	0.0045	0.4115	0.6025	0.0063	0.1781
C_{11}	0.0207	0.4582	0.0258	0.4750	0.0298	0.0031
C_{12}	0.0318	0.0071	0.0430	0.5656	0.0332	0.0260
C_{13}	0.0002	0.9531	0.0967	0.0384	0.1038	0.3432
C_{14}	0.0005	0.0101	0.0070	0.1011	0.0420	0.2622
C_{15}	0.0007	0.1135	0.0580	0.0172	0.0147	0.0006
C_{16}	0.8189	0.4682	0.8249	0.6217	0.1711	0.0371
C_{17}	0.7649	0.5000	0.6897	0.8537	0.0769	0.2885
C_{18}	0.1299	0.8362	0.6595	0.5325	0.3079	0.1662
C_{19}	0.0845	0.6659	0.5401	0.8495	0.1938	0.2591
C_{20}	0.4563	0.6451	0.0168	0.7431	0.0088	0.6117
C_{21}	-	-	0.1891	0.0303	0.8195	0.5569
C_{22}	-	-	0.032	0.3963	0.06325	0.0042

C_{23}	-	-	0.7656	0.2488	0.0062	0.8537

All the coefficient shown in Table 13 proved to be significant at least for one of the outputs studied in this paper so as a matter of simplifying the calculations, they were all kept. In order to show the fit of the surfaces compared to the original data, Table 14 shows the R^2 values.

Table 14 R^2 values for the surfaces obtained for every output in Stage 1

Output	P_{max}	dP/da	NO_x	Smoke	ISFC	CA90abs
R^2	0.9888	0.9409	0.9918	0.9838	0.9975	0.9986

It can be seen that, except for the pressure gradient that shows a lower fitting level than the other, all the surfaces can accurately predict the values of the original DOE points.

The mathematical model used to correlate the optimized input and the outputs of the Stage 2 are shown below.

$$Output = C_1 + db*C_2 + k*C_3 + P2*C_4 + EGR*C_5 + IP*C_6 + SoI_m*C_7 + db^2*C_8 + k^2*C_9 + P2^2*C_{10} + EGR^2*C_{11} + IP^2*C_{12} + SoI_m{}^2*C_{13} + P2*IP*C_{14} + P2*EGR*C_{15} + P2*SoI_m*C_{16} + P2*db*C_{17} + P2*k*C_{18} + EGR*IP*C_{19} + EGR*SoI_m*C_{20} + EGR*db*C_{21} + EGR*k*C_{22} + IP*SoI_m*C_{23} + IP*db*C_{24} + IP*k*C_{25} + SoI_m*db*C_{26} + SoI_m*k*C_{27} + db*k*C_{28} + db^3*C_{29} + k^3*C_{30} + P2^3*C_{31} + EGR^3*C_{32} + MSN^3*C_{33} + SoI_m{}^3*C_{34} + db2*k*C_{35} + db*IP*P2*C_{36} + db*k*P2*C_{37} + db*k*EGR*C_{38} + db*k*IP*C_{39} + db*k*SoI_m*C_{40} + EGR*IP*SoI_m*C_{41} + EGR*P2*k*C_{42} + db2*P2*C_{43} + P2*IP*k*C_{44} + P2*IP*SoI_m*C_{45} + P2*k*SoI_m*C_{46} + db2*k2*C_{47} + db*k*IP*SoI_m*C_{48} + db*k*IP*P2*C_{49} + db*k*IP*EGR*C_{50}$$

Where the inputs db, k, P2, EGR, IP and SoI_m as calculated as the example below.

$$db = (db_{value} - (db_{max} + db_{min}) / 2) / ((db_{max} - db_{min}) / 2)$$

The coefficients C_1 to C_{50} are described in Table 15.

Table 15 RSM coefficients for the Stage 2 optimization.

	Mathematical fit coefficients					
Output	P_{max}	dP/da	NO_x	Smoke	ISFC	CA90abs
C_1	120.017	4.454	149.017	0.485	185.110	393.201
C_2	0.016	-0.040	-29.074	4.132	5.690	6.148
C_3	2.220	-0.022	24.229	0.284	0.186	-1.707
C_4	4.323	0.122	12.870	-0.294	-2.336	-1.322
C_5	-2.108	-0.150	-90.032	0.745	2.467	2.076

C_6	3.742	0.110	12.108	0.817	-0.892	-1.576
C_7	-16.124	0.007	-31.926	-0.698	4.501	2.818
C_8	-0.793	0.056	-35.064	2.079	5.223	7.165
C_9	-0.290	0.054	-26.282	1.487	3.123	4.153
C_{10}	-0.093	0.051	-2.743	0.432	0.190	0.037
C_{11}	-0.190	0.060	6.215	0.292	0.348	0.229
C_{12}	-0.115	0.051	-2.924	0.117	0.156	0.191
C_{13}	2.105	0.032	1.256	0.610	0.571	0.088
C_{14}	0.061	-0.006	1.561	0.084	-0.053	-0.031
C_{15}	0.100	-0.031	0.401	-0.179	-0.528	-0.306
C_{16}	-0.540	0.008	-3.760	0.120	0.070	0.035
C_{17}	0.191	0.003	1.728	-1.926	-1.543	-0.728
C_{18}	-0.041	-0.019	3.879	0.152	-0.527	-0.487
C_{19}	-0.302	0.039	-5.705	0.021	-0.099	-0.160
C_{20}	0.414	0.001	10.982	-0.117	0.072	0.089
C_{21}	0.506	-0.032	17.965	1.574	1.045	0.223
C_{22}	-0.321	-0.016	-9.766	0.149	0.113	-0.054
C_{23}	-0.772	-0.016	-1.329	0.126	-0.507	-0.232
C_{24}	-1.044	-0.029	-14.468	2.219	1.923	1.240
C_{25}	0.780	-0.003	-3.073	-0.584	1.119	1.162
C_{26}	0.631	-0.001	20.299	-2.074	-2.873	-2.897
C_{27}	-0.129	-0.005	6.356	0.021	-2.061	-1.948
C_{28}	-2.940	-0.010	-65.452	4.177	7.212	8.576
C_{29}	2.071	0.011	36.321	-2.335	-4.346	-4.082
C_{30}	-0.529	0.008	-5.271	1.339	-0.564	-0.674
C_{31}	0.008	0.015	3.204	-0.506	-0.009	0.024
C_{32}	0.142	0.010	8.861	-0.057	-0.003	0.000
C_{33}	-0.413	0.031	-0.448	-0.435	-0.007	0.148
C_{34}	2.327	-0.021	0.582	-0.256	-0.368	-0.221
C_{35}	-	-	-	7.720	-	-
C_{36}	-	-	-	0.310	-	-
C_{37}	-	-	-	0.759	-	-
C_{38}	-	-	-	0.223	-	-
C_{39}	-	-	-	-2.115	-	-
C_{40}	-	-	-	0.979	-	-
C_{41}	-	-	-	0.354	-	-

C_{42}	-	-	-	0.406	-	-
C_{43}	-	-	-	-2.684	-	-
C_{44}	-	-	-	0.488	-	-
C_{45}	-	-	-	-0.587	-	-
C_{46}	-	-	-	-0.653	-	-
C_{47}	-	-	-	1.517	-	-
C_{48}	-	-	-	25.523	-	-
C_{49}	-	-	-	1.793	-	-
C_{50}	-	-	-	-2.335	-	-

A study of the significance level of the coefficients was performed. The results from the ANOVA for each coefficient is shown in Table 16.

Table 16 P-value for all the coefficients used in the RSM for Stage 2

	P-values for all coefficients					
Output	P_{max}	dP/da	NO_x	Smoke	ISFC	CA90abs
C_1	0.0000	0.0000	0.0000	0.0000	0.0000	0.0000
C_2	0.0000	0.0000	0.0000	0.0000	0.0000	0.0000
C_3	0.0000	0.0091	0.0000	0.0000	0.0000	0.0000
C_4	0.0000	0.0000	0.0000	0.0000	0.0000	0.0000
C_5	0.0000	0.0000	0.0000	0.0000	0.0000	0.0000
C_6	0.0000	0.0000	0.0000	0.0000	0.0000	0.0000
C_7	0.0000	0.0230	0.0000	0.0000	0.0000	0.0000
C_8	0.5700	0.6420	0.0398	0.4825	0.0747	0.0127
C_9	0.1705	0.2001	0.0329	0.5237	0.0000	0.0185
C_{10}	0.6505	0.5300	0.0000	0.3154	0.0000	0.1019
C_{11}	0.0245	0.5276	0.2360	0.0587	0.5424	0.0000
C_{12}	0.1376	0.2663	0.1135	0.0000	0.5721	0.6085
C_{13}	0.0176	0.3975	0.0556	0.6393	0.6081	0.4058
C_{14}	0.1405	0.9186	0.0000	0.6269	0.2372	0.0011
C_{15}	0.0309	0.0329	0.0575	0.3139	0.0000	0.0000
C_{16}	0.0000	0.6125	0.0000	0.4784	0.1610	0.0001
C_{17}	0.0013	0.6125	0.0000	0.0000	0.0000	0.0000
C_{18}	0.3005	0.1559	0.0000	0.3973	0.0000	0.0000
C_{19}	0.0001	0.0243	0.0000	0.8713	0.0664	0.5043
C_{20}	0.0000	0.7598	0.0000	0.5138	0.1373	0.0021
C_{21}	0.0000	0.0613	0.0000	0.0000	0.0000	0.0000

C_{22}	0.0001	0.2106	0.0000	0.3973	0.0443	0.0000
C_{23}	0.0000	0.2818	0.0001	0.4613	0.0000	0.0001
C_{24}	0.0000	0.0449	0.0000	0.0000	0.0000	0.0000
C_{25}	0.0000	0.7598	0.0000	0.0092	0.0000	0.0000
C_{26}	0.0000	0.9186	0.0000	0.0000	0.0000	0.0000
C_{27}	0.0103	0.7598	0.0000	0.8945	0.0000	0.0000
C_{28}	0.0000	0.2818	0.0000	0.0000	0.0000	0.0000
C_{29}	0.0431	0.0531	0.2179	0.1067	0.0591	0.3849
C_{30}	0.3313	0.0378	0.0370	0.5781	0.2798	0.1015
C_{31}	0.2462	0.3716	0.1160	0.3768	0.0182	0.5971
C_{32}	0.5816	0.5454	0.4214	0.6973	0.5600	0.0435
C_{33}	0.0410	0.6538	0.0184	0.0547	0.3020	0.2457
C_{34}	0.3848	0.0909	0.0458	0.3099	0.6375	0.3593
C_{35}				0.0081		
C_{36}				0.0522		
C_{37}				0.0142		
C_{38}				0.0063		
C_{39}				0.0026		
C_{40}				0.0463		
C_{41}				0.0469		
C_{42}				0.0421		
C_{43}				0.0021		
C_{44}				0.0333		
C_{45}				0.025		
C_{46}				0.0194		
C_{47}				0.1311		
C_{48}				0.0289		
C_{49}				0.021		
C_{50}				0.011		

All the coefficient shown in Table 16 proved to be significant at least for one of the outputs studied in this paper so as a matter of simplifying the calculations, they were all kept. In order to show the fit of the surfaces compared to the original data, Table 17 shows the R^2 values.

Table 17 R^2 values for the surfaces obtained for every output in Stage 1

Output	P_{max}	dP/da	NO_x	Smoke	ISFC	CA90abs
R^2	0.9981	0.9597	0.998	0.9904	0.9978	0.9934

It can be seen that, except for the pressure gradient that shows a lower fitting level than the other, all the surfaces can accurately predict the values of the original DOE points.